Thermodynamics of the Dimer−Decamer Transition of Reduced Human and Plant 2-Cys Peroxiredoxin[†]

Sergio Barranco-Medina,[‡] Sergej Kakorin,[§] Juan José Lázaro,[||] and Karl-Josef Dietz*[,‡]

Biochemistry and Physiology of Plants, Faculty of Biology-W5, Bielefeld University, 33501 Bielefeld, Germany, Biophysical Chemistry, Faculty of Chemistry-F3, Bielefeld University, D-33501 Bielefeld, Germany, and Department of Biochemistry and Cellular and Molecular Biology of Plants, Estación Experimental del Zaidín, Consejo Superior de Investigaciones Científicas, E-18008 Granada, Spain

Received February 20, 2008; Revised Manuscript Received April 17, 2008

ABSTRACT: Isothermal titration calorimetry (ITC) is a powerful technique for investigating self-association processes of protein complexes and was expected to reveal quantitative data on peroxiredoxin oligomerization by directly measuring the thermodynamic parameters of dimer−dimer interaction. Recombinant classical 2-cysteine peroxoredoxins from *Homo sapiens*, *Arabidopsis thaliana*, and *Pisum sativum* as well as a carboxy-terminally truncated variant were subjected to ITC analysis by stepwise injection into the reaction vessel under various redox conditions. The direct measurement of the decamer−dimer equilibrium of reduced peroxiredoxin revealed a critical concentration in the very low micromolar range. The data suggest a cooperative assembly above this critical transition concentration where a nucleus facilitates assembly. The rather abrupt transition indicates that assembly processes do not occur below the critical transition concentration while oligomerization is efficiently triggered above it. The magnitude of the measured enthalpy confirmed the endothermic nature of the peroxiredoxin oligomerization. Heterocomplexes between peroxiredoxin polypeptides from different species were not formed. We conclude that a functional constraint conserved the dimer−decamer transition with highly similar critical transition concentrations despite emerging sequence variation during evolution.

Peroxiredoxins (PRXs)[1] exist in all analyzed organisms. Their peroxidase activity depends on at least one Cys residue in the catalytic center (*1, 2*). Their classification is based on sequence similarities and the mechanism used to re-reduce the oxidized catalytic Cys (*3*). Many studies have shown their implication in different diseases such as cancer, apoptosis, and malaria (*4–6*), underlining the outstanding role of PRXs. Since the first transmission electron microscopy observation of PRXs as a doughnutlike oligomer (*7*), the function and dynamics of PRX oligomerization have been addressed in several studies but remained partly elusive. With the exception of PRX Q, e.g., from *Saccharomyces cerevisiae* and plants, that exists as a monomer, PRXs are obligate dimers with a strong tendency to form higher-order oligomers, particularly decamers and dodecamers. Their oligomeric state depended on pH and ionic strength (*8–11*). Crystallographic structure analysis of more than 35 different PRXs has resolved the interface characteristics of these proteins and established the structure−function relationship during the catalytic cycle.

The minimum functional unit is the 2-CysPRX dimer which enables the formation of disulfide bonds between the catalytic and peroxidatic cysteine residues of the two subunits (*2, 12*). The 2-CysPRX dimers have a strong tendency to assemble to ordered oligomers with a doughnutlike shape. The oligomeric state of the protein is linked to its redox state with dimerization being favored under oxidizing and decamerization under reducing conditions (*12, 13*).

The resolved crystal structures of different 2-CysPRXs demonstrated that the oxidized form usually is an α_2 dimer, whereas the reduced form exists as an $(\alpha_2)5$ decamer (*14, 15*). The monomer−monomer and dimer−dimer interactions are stabilized by B-type interfaces with the β-sheets of the two monomers in a parallel orientation and A-type interfaces with a perpendicular orientation of the β-sheets, respectively (*16*). The dynamic assembly−disassembly process occurs in a functional context. In its reduced form, i.e., with a reduced peroxidatic (C_p) and a resolving cysteine (C_R) residue, the structure of 2-CysPRX is fully folded. The reaction with the peroxide substrate oxidizes the C_p to sulfenic acid which is protected in the active site pocket by the first turn of helix α_2. To enable the attack and reduction of C_p, a partial unfolding of the structure by movement of helix α_2 is needed to form the "C_p loop" (*12*). At this stage, the new intermediate is represented by the partially unfolded PRX in dynamic equilibrium with the fully folded PRX. Finally, the disulfide

[†] This work was supported by the DFG (Di 346) and by the SFB 613.

* To whom correspondence should be addressed: Biochemistry and Physiology of Plants, Faculty of Biology-W5, Bielefeld University, 33501 Bielefeld, Germany. Telephone: +49 521 106 5589. Fax: +49 521 106 6039. E-mail: karl-josef.dietz@uni-bielefeld.de.

[‡] Faculty of Biology-W5, Bielefeld University.

[§] Department of Chemistry-F3, Bielefeld University.

[||] Consejo Superior de Investigaciones Científicas.

[1] Abbreviations: CTC, critical transition concentration; DTT, dithiothreitol; ITC, isothermal titration calorimetry; PRDX1, human PRX1; PRX, peroxiredoxin.

10.1021/bi8002956 CCC: $40.75
Published on Web 06/14/2008

bridge is formed and the oxidized PRX locked in the partially unfolded state. The reduced active state is regenerated by reduction using thiol donors such as thioredoxins, glutaredoxins, or cyclophilins (*1, 17*). Under highly oxidizing conditions, C_p may become overoxidized to sulfinic or sulfonic acid. The overoxidized form partly mimics the reduced state (*18*). Irrespective of some contradicting reports in relation to the effect of pH and ionic strength on oligomerization (*19–21*), it is largely accepted that the oligomeric state of 2-CysPRX is redox sensitive (*12, 22*).

Despite recent progress in understanding the redox-dependent dimer−oligomer transition and structure, the dynamics of assembly and disassembly has not been clarified until now. Thermodynamic tools such as microthermocalorimetry offer innovative approaches to the PRX oligomerization process. In biochemistry, protein−ligand, protein−protein, protein−DNA, or protein−RNA interactions can be studied if the net thermodynamic effects of molecular interaction are sufficiently large. The obtained data enable us to determine the stoichiometry, the formation enthalpy, and the binding constant of these complexes. Consequently, the Gibbs free energy of the compound can be calculated and subsequently the entropy of the process (*23*). In principle, most interactions release or absorb heat. The heat change is measured directly in solution and under constant pressure; thus, the true enthalpy of the ongoing reaction is measured directly. These characteristics make ITC superior to methods that indirectly measure enthalpic changes, e.g., based on the dependence of the association constant on temperature (vant Hoff's equation) and obtained with techniques like ultrafiltration or exclusion chromatography (*24, 25*).

ITC dilution experiments were conducted to investigate dissociation processes such as dimer−monomer or oligomer−monomer transitions or the assembly of micelles with antibiotics or proteins (*26–30*). Proteins initially present at high concentrations are injected in the buffer present in the adiabatic cell. If the proteins disassemble, the disintegration is coupled to the release or uptake of heat. As the protein concentration increases in the calorimetric cell, the dissociation is less favored. Beyond a certain concentration, the dissociation ceases and only heat dilution is detected upon further injections. This gives rise to a typical heat dilution curve allowing the calculation of the enthalpy, entropy, and equilibrium constant (*27*). Considering a total macromolecule concentration ($[M]_T$) in the calorimetric cell, the dissociation constant determines the partitioning between the different species, in the case of the 2-CysPRX between dimers ($[M_2]$) and decamers ($[M_{10}]$), equivalent to a decamer−five-dimer dissociation. The K_d is calculated according to the equation

$$K_d = [M_2]^5/[M_{10}] \quad (1)$$

It will be shown that this model describing a dissociation equilibrium between the dimer and the decamer does not adequately describe the observed sharp transition between both molecular species of 2-CysPRX.

The heat released (q_i) or absorbed in each injection is proportional to the increment of the concentration of dimer ($[M_2]$) in the cell after injection *i*.

$$q_i = V\Delta H_d([M_2] - [M_2]_{i-1} - F_0[M_2]_0 v/V) \quad (2)$$

where V is the cell volume, v is the injection volume, ΔH_d is the dissociation enthalpy (per dimer), F_0 is the fraction of dimer in the concentrated solution in the syringe, and $[M_2]_0$ is the initial total concentration of the macromolecule (as dimer) in the syringe. The second term in the equation accounts for the increment of dimer concentration in the cell due to the addition of possible dimers from the syringe (*31*). In addition, the calculation must take into account the dilution with each injection.

The aim of the study was to assess the dissociation properties of the ubiquitously occurring 2-CysPRX. ITC dilution assays with PRXs from different species as well as with the truncated protein have been performed. The results provide a first thermodynamic approximation of the PRX oligomerization phenomenon and advance our understanding of the physiological role of PRX oligomers in vivo.

EXPERIMENTAL PROCEDURES

Protein Preparation. (i) Protein Electrophoresis. Nonreducing denaturing SDS−PAGE was performed with 6% (w/v) stacking and 15% (w/v) resolving polyacrylamide gels stained with Coomassie Brilliant Blue (*10*).

(ii) Cloning and Purification of Recombinant Ps-2-CysPRX without a His Tag. A cDNA encoding the mature protein from pea (GenBank accession number AJ315851) without the chloroplast transit peptide was cloned into pET3d using NcoI and BamHI restriction enzymes and transformed in BL21 *Escherichia coli* (DE3). Protein was expressed at 37 °C by addition of IPTG (0.4 mM). After induction for 6 h, cells were sedimented, resuspended, and disrupted with a French press. Recombinant pea PRX was purified by subsequent passage through Sephacryl S-200 gel filtration, Mono Q HR 5/5 ion exchange, and Phenyl Superose HR 5/5 columns (GE Healthcare, Uppsala, Sweden) (*9*).

(iii) Cloning and Purification of Recombinant His-Tagged Protein. Proteins were generated as recombinant proteins in *E. coli* using the pQE vector (*8*). The C-terminally truncated variant of At-2-CysPRX was cloned with the following primers: 5′-gcagaggctgtgtttgat-3′ (forward), 5′-tcagacttcatccgggtt-3′ (reverse), the human PRDX1 with the primer combination hPrxI-*Bam*HI-F(5′-aaaaggatccaatgtcttcaggaaatgct-3′)/hPrxI-AgeI-R(*5′-ttttaccggtcacttctgcttggagaa-3′). Following IPTG-induced expression, proteins were purified by being bound to Ni-nitriloacetic acid Sepharose and following washing eluted with imidazole.

(iv) Dialysis and Quantification. Prior to ITC experiments, the proteins were extensively dialyzed against buffer containing 40 mM phosphate (pH 8.0) and 1 mM DTT at 4 °C overnight (no DTT in the experiment with oxidized protein). All solutions were filtered through a 0.22 μm filter (Rothman) and degassed before the titrations.

Isothermal Titration Calorimetry. Isothermal titration calorimetry (ITC) was performed with a VP calorimeter (Microcal, Northampton, MA). The mixing cell had a volume of 1.4 mL. To prevent large proton ionization heats, ITC experiments were performed in phosphate buffer with a low ionization enthalpy (ΔH^{ion}) of 0.9 kcal/mol in which PRXs are stable. Protein concentrations were measured by reading the absorbance at 280 nm (Nano-Drop system). The reference power was set to 10 μcal/s, and the cell contents were stirred at 270 rpm throughout the titrations at 25 °C. After an initial 60 s delay, series of 1.6−9 μL (as indicated) of protein solution were injected into the cell containing buffer only.

A 3 min time interval was chosen to allow formation of an equilibrium after each injection. The first injection was an incomplete injection and was ignored during data analysis. The background heat from dilution was estimated from the integral of the peaks observed after the critical transition concentration (CTC) had been surpassed.

Data were analyzed using the software provided by MicroCal Systems. Each peak in power (microcalories per second) versus time plot was integrated and normalized to yield molar enthalpies for each injection.

Adjustment of Redox States. To adjust the redox state of At-2-CysPRX in the reduced state (SH) or oxidized state (S−S), the protein was incubated with 50 μM H_2O_2 or 10 mM DTT in phosphate buffer (40 mM, pH 8.0), respectively, and dialyzed at 4 °C overnight.

The overoxidized state (SOOH) was obtained by incubation with 10 mM DTT for 15 min and subsequent addition of 50 mM H_2O_2 for 1 h. The protein was dialyzed overnight against phosphate buffer (40 mM, pH 8.0) at 4 °C with DTT (reduced protein injected into a solution of the overoxidized form) or without DTT for the normal dilution experiments.

Gel Filtration Analysis. The aggregation of recombinant His-tagged At-2-CysPRX was explored by gel filtration on a Superose 12 column (GE Healthcare) equilibrated in KP_i buffer (40 mM, pH 8.0) with a flow rate of 0.5 mL/min. The elution of the 200 μL of injected protein was monitored at 280 nm after loading (*32*).

RESULTS

ITC dilution experiments with 2-CysPRX were performed to determine the thermodynamic parameters of its self-assembly. Typically, the injection syringe is filled with a protein solution at a concentration 20-fold higher than the critical concentration (CC). The term critical concentration is derived from micelle formation observed in detergent solutions once a critical concentration is surpassed (*33*). To distinguish the process described during the PRX dimer−decamer transition with its defined stochiometry from micelle formation with a nonfixed stoichiometry, the term critical transition concentration (CTC) is used throughout the text. The injection into the calorimeter cell containing buffer leads to several hundred-fold dilution. If the resulting concentration in the cell is significantly less than the CTC, the injected oligomers disintegrate into monomers or dimers, a process accompanied by release of heat. The heat changes are quantified by a power-compensation feedback mechanism in the machine.

Formation of PRX decamers was maximized by adjusting reducing conditions with DTT in the buffer (*9, 12*). PRX was diluted inside the microcalorimeter cell from a concentration where it predominantly existed as decamer to a concentration where it preferentially forms dimers. The initial dilution experiments were carried out with 6 μL injections of *Arabidopsis thaliana* 2-CysPRX at a monomer concentration of 50 μM. The first injections resulted in PRX decamer dissociation with concomitant heat generation, but after a few injections, a sudden change in response occurred and only background heat dilution was seen (data not shown). The oligomerization midpoint or CTC defines the transition point at which half of the injected decamers dissociate. Above the CTC, the injected enzyme does not dissociate and the peaks approach the level of heat dilution. Due to the very abrupt transition, the precise CTC could not be derived from these experiments but was estimated to be between 1 and 2 μM monomer. To accurately identify the transition, a refined ITC dilution experiment was performed with decreased injection volumes of 1.6 μL (Figure 1A). As expected, more injections were needed to reach the CTC. The heat peaks were integrated and normalized with respect to the molar amount of PRX injected and plotted versus the monomer PRX concentration in the cell, yielding a CTC of 1.52 μM (mean of seven measurements). The heat of dissociation was estimated using the dimer−monomer model provided by MicroCal. The average of the integrated heat generation (kilocalories per mole) of all points before the sharp transition (except the peak from the first injection) was 142 ± 24 kcal/mol of dimer calculated according to eq 3.

$$\Delta H_d = \Delta H_m \frac{c_m}{c_d} \quad (3)$$

where ΔH_d is the enthalpy per mole of dimer, ΔH_m is the measured value per mole of monomer, and c_m and c_d reflect the molar conversion factors. The average ΔH_m from seven determinations was 71 ± 12.

To elucidate whether PRXs from other species respond in a similar manner, recombinant Ps-2-CysPRX from pea without the His tag, Hs-PRDX1, and monomeric At-PRX Q were analyzed as well. The serial injection of reduced His-tagged free Ps-2-CysPRX allowed us to calculate the CTC of 0.9 μM ($n = 2$) (Figure 1B) and the association enthalpy of 135 kcal/mol of dimer. The CTC for human PRDX1 was 1.3 μM ($n = 2$) with an enthalpy assembly value of 156 kcal/mol of dimer (Figure 1C). As expected, injections of monomeric At-PRX Q did not result in protein dissociation, and only the heat of dilution was observed (Figure 1D).

To test for the oligomeric state of the reduced form, At-2-CysPRX as used in the syringe was passed through a Superdex column (Figure 2) and shown to be in the oligomeric form at a concentration of 50 μM. The monomeric molecular mass is 21.3 kDa.

Interface size, geometric complementarity, and amino acid hydrophobicity and polarity influence protein binding efficiency (*34*). In the case of PRX, Parsonage et al. (*35*) observed that mutations of Thr77 at the decamer-building interface of AhpC from *Salmonella typhimurium* (variants T77I and T77D) disrupted the decamer. This was accompanied by a 100-fold decrease in peroxidase activity, while the T77V variant stabilized the decamer. All typical 2-CysPRXs contain the resolving cysteine C_R in a B-sheet near the C-terminal domain of the polypeptide. This domain unfolds to allow the exposition of C_R. To study the function of the carboxy-terminal domain of At-2-CysPRX in the oligomerization reaction, a truncated protein lacking the last 26 amino acids (including C_R) was subjected to ITC dilution assays and behaved in a manner quite similar to that of the wild-type protein (data not shown) with a CTC of 1.75 μM. The heat of binding was 195 ± 35 kcal/mol of dimer.

The redox state is crucial for the oligomeric state of 2-CysPRX. The redox state of the proteins was adjusted and tested by nonreducing SDS−PAGE (Figure 3). Oxidized At-2-CysPRX separated as dimer, indicating the presence of the intermolecular disulfide bond, whereas the overoxidized PRX

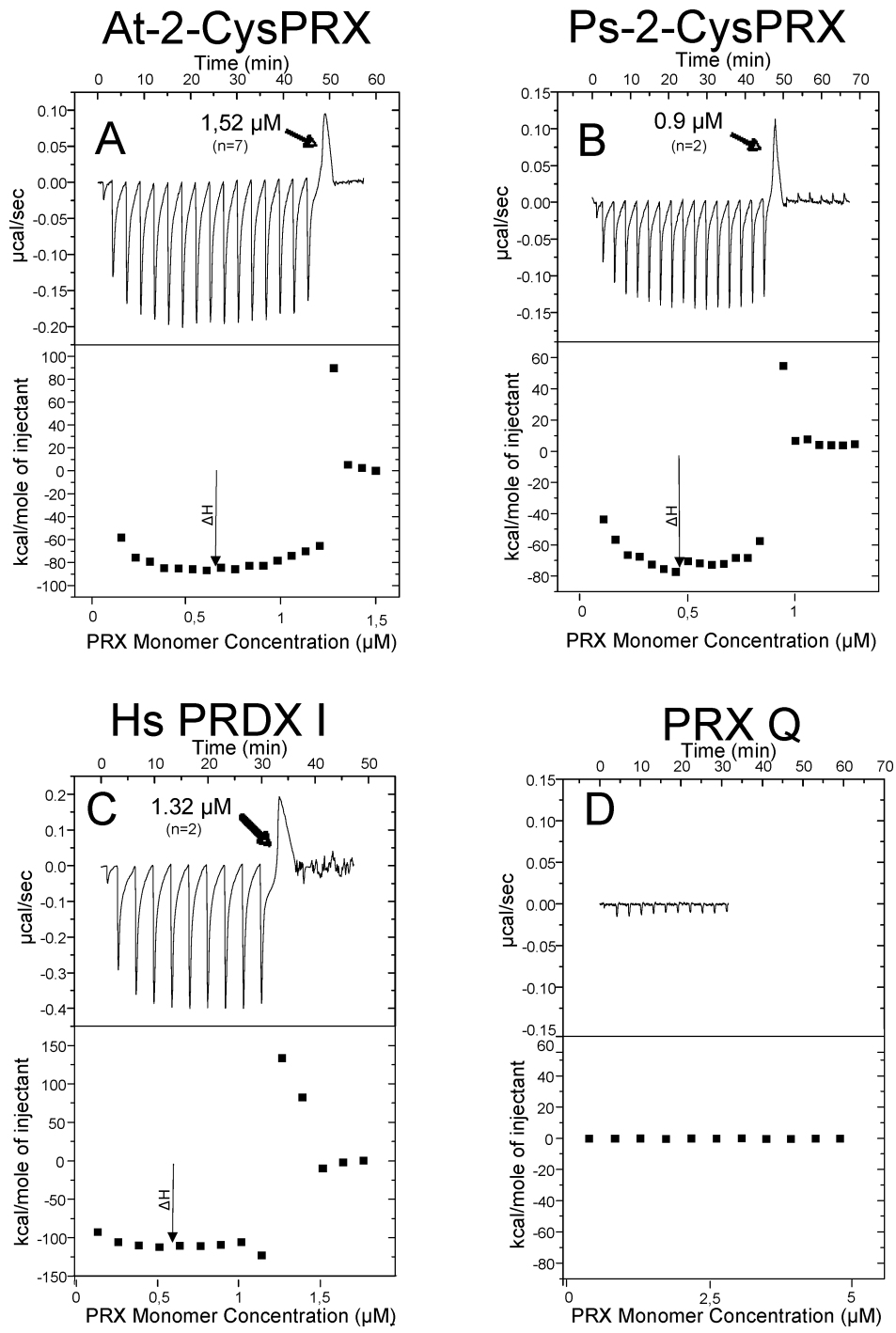

FIGURE 1: Calorimetric dilution experiments for exothermic dissociation of recombinant PRX decamers at pH 8.0. The top panels present the raw data for a series of 1.6 μL injections of At-2-CysPRX at a monomer concentration of 70 μM (A), *Pisum sativum* His-tag free 2-CysPRX at 50 μM (B), and *Homo sapiens* PRDX1 at 102 μM (C) and 9 μL injections of At-PRX Q at 70 μM (D) into KP_i buffer (40 mM) supplemented with 1 mM DTT at 25 °C. The bottom panels show the integrated injection heat values, corrected for the control heat with the dissociation model and represented as the function of PRX monomer concentration in the cell. The given CTC values were derived from the abrupt transition and are given as averages from *n* independent ITC dilution assays.

migrated as monomer (21.3 kDa) and was unable to form disulfide bridges under oxidizing conditions. As revealed by ITC measurements, oxidized and overoxidized At-2-CysPRX at 50 μM did not release heat upon injection in the cell (Figure 3).

To assess the interaction of the overoxidized with the reduced form, the overoxidized enzyme was incubated with 5 mM DTT and dialyzed overnight in buffer containing 1 mM DTT. Reduced At-2-CysPRX at 120 μM was injected into the cell containing the DTT-treated overoxidized protein at 10 μM, i.e., a concentration far greater than the CTC. As depicted in Figure 3C, reduced At-2-CysPRX dissociated when injected into the overoxidized enzyme under reducing conditions with a CTC of 1.61 μM. This finding shows that the overoxidized At-2-CysPRX did not interact with the reduced form.

The complementarity of PRX interfaces from different sources was studied by injecting At-2-CysPRX into human PRDX1, Ps-2-CysPRX, or albumin as a control (Figure 4). If the dimer−dimer interface were conserved among the

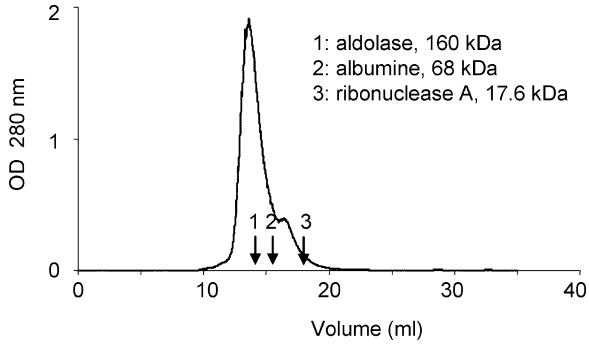

FIGURE 2: Elution profile of At-2-CysPRX after size exclusion chromatography through Superose 12 as monitored at 280 nm. The column was calibrated with standard proteins as indicated.

different PRXs, the expected number of injections required to arrive at the CTC should be smaller than in a normal At-2-CysPRX/buffer experiment. However, the presence of the heterologous PRX protein in the cuvette did not affect the dissociation behavior of the injected At-2-CysPRX (Figure 4A). Apparently, the PRX interfaces were not sufficiently conserved during evolution despite highly similar CTCs. Figure 4B shows the amino acid alignment of the three typical 2-CysPRXs used in this study with the four main regions (highlighted in gray) implicated in the dimer−dimer interface to form decamers as described by Wood et al. (*12*). The amino acid variability between *Arabidopsis* and *H. sapiens* (six of a total of 24 amino acids are different) provides substantial changes in the interface impeding the coupling of mixed At-2-CysPRX−Hs-2-CysPRDX1 interfaces to form decamers. Apparently, a specific differentiation between 2-CysPRX occurred during evolution. Interestingly, despite the high level of identity (22 of 24 identical) of the four regions between pea and *Arabidopsis* 2-CysPRX, the dissociation pattern of the injected At-2-CysPRX also remained unchanged after injection of the enzyme into Ps-2-CysPRX, proving that a heterocomplex is not formed (data not shown).

In a modified approach and to exclude artifacts, At-2-CysPRX was injected into the cuvette preloaded with the same protein with a monomer concentration of 0−50 μM. Injections into 2-CysPRX solutions at concentrations below the CTC should give enthalpic responses, while above the CTC, the responses would approach the background level. The values of integrated peaks per mole of the first four peaks (in kilocalories per mole) from three independent ITC dilutions were averaged for each 2-CysPRX concentration. Figure 5A shows the elaborated thermogram with a plot of the heat values with inverted sign (*y*-axis) against the 2-CysPRX concentration in the cell in the range between 0 and 2 μM dimer (*x*-axis, corresponding to 0−4 μM monomer). Injection of 50 μM 2-CysPRX into the cell filled with the same solution gave little heat release (not shown). In a converse manner, the dilution of the same 2-CysPRX solution into plain buffer produced maximal heat. As in the initial dilution experiments, the transition was abrupt and was characterized by only one transition point corresponding to the cell concentration of 1.58 μM. A very small decrease in the cell concentration, for example, to 1.55 μM enabled an almost complete disassembly, whereas tiny increases in the 2-CysPRX concentration to 1.6 μM inhibited dissociation. Apparently, the method of 2-CysPRX addition (Figure 5) and the titration experiment (Figure 1) gave similar estimates of the CTC. The observed difference of 0.06 μM is in the range of accuracy of the protein concentration determination.

MODELING OF THE TRANSITION

In the more general case of the *n*-dimer−dimer dissociation according to

$$n\mathrm{M}_2 = \mathrm{M}_{2n} \tag{4}$$

the dissociation constant K_d for the partitioning between the dimers, $[M_2]$, and *n*-dimers, $[M_{2n}]$, is given by

$$K_d = [\mathrm{M}_2]^n/[\mathrm{M}_{2n}] \tag{5}$$

where *n* is the stoichiometric coefficient.

Applying the mass conservation law

$$[\mathrm{M}_2]_T = [\mathrm{M}_2] + n[\mathrm{M}_{2n}] \tag{6}$$

to eq 4, we derive the equation for the equilibrium concentration of free dimers ($[M_2]$):

$$n[\mathrm{M}_2]^n + K_d[\mathrm{M}_2] - K_d[\mathrm{M}_2]_T = 0 \tag{7}$$

When $n > 3$, eq 6 can be solved numerically only, for instance, with Mathcad. Solution of eq 6 yields $[M_2]$ as a function of the total concentration ($[M_2]_T$) of dimers in the cell. It is recalled that the dimers are injected into the cell in the form of *n*-dimers. At many-fold dilution, the *n*-dimers rapidly dissolve into dimers. Dissociation of the *n*-dimers causes an exothermic heat, δh, proportional to the increase in the amount, δn_2, of dimers dissociated from the *n*-dimers. The ratio $\delta h/\delta(n_2)_T$ is proportional to $\delta[M_2]/\delta[M_2]_T$, where $\delta(n_2)_T$ is the total amount of injected dimers and $\delta[M_2]$ and $\delta[M_2]_T$ are the differential increases in the free and total concentrations of dimers, respectively. For further analysis, we define the grade θ of the transition between *n*-dimers and dimers

$$\theta = \frac{\delta h/\delta(n_2)_T}{[\delta h/\delta(n_2)_T]_{max}} = \frac{\delta[\mathrm{M}_2]/\delta[\mathrm{M}_2]_T}{(\delta[\mathrm{M}_2]/\delta[\mathrm{M}_2]_T)_{max}} \tag{8}$$

where the index max denotes the maximum value of the $\delta h/\delta(n_2)_T$ and $\delta[M_2]/\delta[M_2]_T$ ratios, respectively. Clearly, the maximum value of $\delta[M_2]/\delta[M_2]_T$, corresponding to the complete dissociation of *n*-dimers into dimers, is always 1 [$(\delta[M_2]/\delta[M_2]_T)_{max} = 1$]. Since the aliquots, $\delta(n_2)_T$, of the *n*-dimers injected into the cell are always equal, the ratio (*8*) simplifies to $\theta = \delta h/\delta h_{max}$. The Mathcad numerical code, fitting the theoretical model $\delta[M_2]/\delta[M_2]_T$ to the experimental data for $\theta = \delta h/\delta h_{max}$ to find the two free parameters *n* and K_d, can be provided on demand. The result of the fit is presented in Figure 5A. The maximum value δh_{max} has been calculated as an average of the first seven measured points. The minimum standard deviation $S = \sqrt{\sum_{i=1}^{N=14}(\delta[M_2]_i/\delta[M_2]_T - 0_i)^2/N} = 0.14$, where $N = 14$ is the number of measured points, is found at the very large stoichiometric coefficient $n = 130 \pm 5$ and the very small macroscopic dissociation constant $K_d = (2.4 \pm 0.2) \times 10^{-10}$ μM^{n-1}. With the constant K_d, the so-called microscopic dissociation constant, k_d (for dimer), is calculated with the relation $k_d = K_d^{1/n} = 0.8 \pm 0.1$ $\mu M^{(n-1)/n}$. The stoichiometric coefficient $n = 130 \pm 5$ suggests that the dissociation of the *n*-dimers is a highly cooperative process, very similar to the demicellization process (*33*). Actually, calculations with eq 6 at $n = 130$ and $K_d = 2.4 \times 10^{-10}$ μM^{n-1} show that the

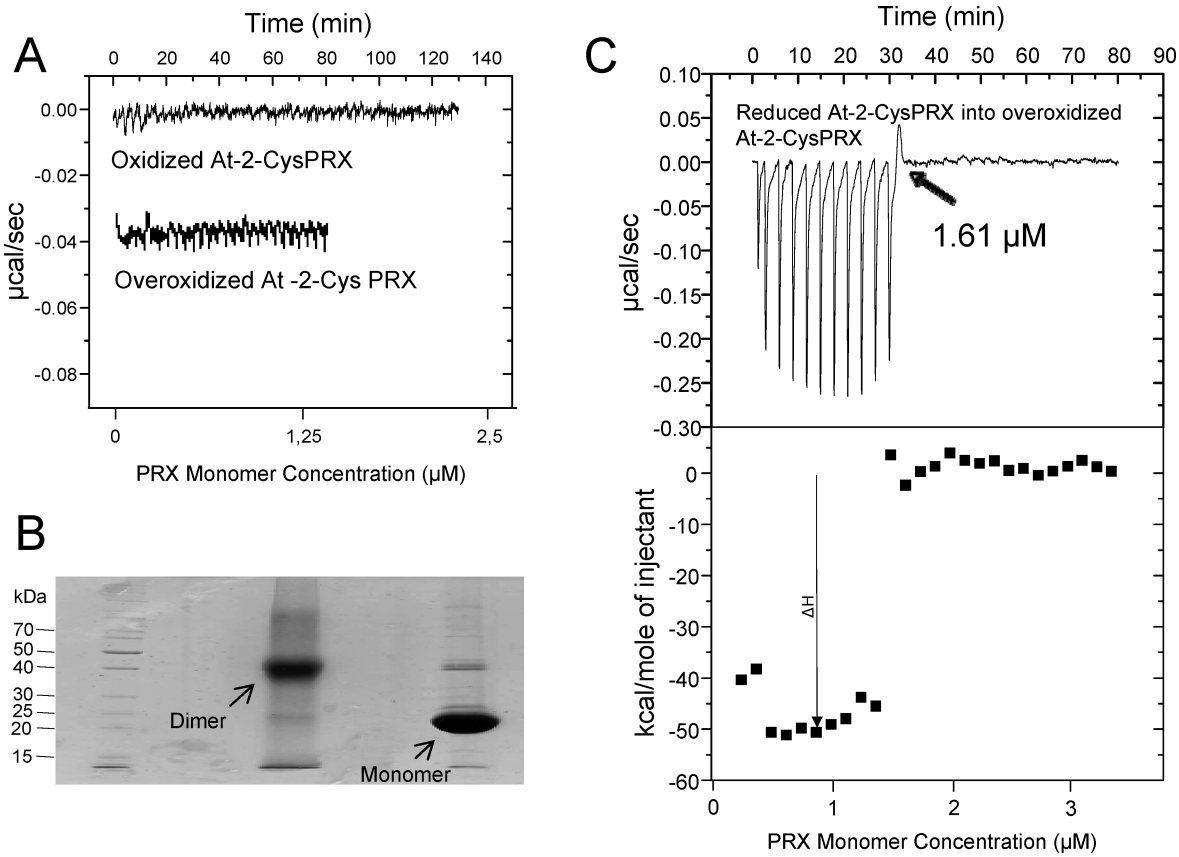

FIGURE 3: Characterization of oxidized and overoxidized At-2-CysPRX. (A) Thermogram of an ITC dilution experiment with oxidized and overoxidized At-2-CysPRX at a monomer concentration of 50 μM. Thermal power is plotted vs time. Only heat dilution is seen after sample injection. (B) Electrophoretic mobility of oxidized (S-S) and overoxidized (SOOH) At-2-CysPRX protein determined via nonreducing SDS−PAGE visualized by Coomassie staining. (C) Oligomer dissociation of reduced At-2-CysPRX (120 μM) after injection into overoxidized At-2-CysPRX (10 μM) as analyzed in an ITC dilution assay. Recombinant protein (1.6 μL) was injected in 40 mM phosphate buffer (pH 7.0) with 1 mmol of DTT/L with a time interval of 180 s between each injection.

concentration of the free dimers ($[M_2]$) first linearly increases with $[M_2]_T$ and then, beginning with the so-called critical micellar concentration of 0.79 μM, approaches the saturation level $[M_2]_{sat} \approx 0.8$ μM (Figure 5B). The equilibrium concentration of the *n*-dimers starts to increase just after the CTC point (Figure 5C). The calculated behavior of the concentrations is typical for the demicellization process. Therefore, we can characterize *n*-dimer−dimer dissociation by the overall critical transition concentration defined as the concentration $[M_2]_T$ at $\theta = 0.5$ according to the relationship CTC $= [M_2]_T(\theta = 0.5) = 0.79 \pm 0.1$ μM (Figure 5A). The observed value of CTC is equal (considering the error margin) to $[M_2]_{sat} \approx 0.8$ μM and to the microscopic dissociation constant $k_d = K_d^{1/n} = 0.8 \pm 0.1$ $\mu M^{(n-1)/n}$, suggesting that the K_d value of 2.4×10^{-10} $\mu M^{n-1}$is calculated correctly. Because $(n - 1)/n = 0.99 \approx 1$, we can neglect small differences between dimensions of CTC and k_d. At T = 293 K (20 °C), the standard free energy of micellization in water is calculated by Heerklotz and Seelig (*33*):

$$\Delta G^0 = RT \cdot \ln\left(\frac{\mathrm{CMC}}{55.5\ \mathrm{M}}\right) = -44\frac{KJ}{mol} \qquad (9)$$

where the constant 55.5 M is the molar concentration of water, CMC = CTC = 0.79 μM and *R* is the gas constant.

DISCUSSION

The data from the ITC dilution experiment show that 2-CysPRX disassembly involves favorable enthalpy (negative). The overall negative value of the Gibbs free energy indicates that the PRX disassembly is a thermodynamically favorable reaction as long as the concentration is less than the CTC. The enthalpy changes of assembly have the same magnitude with opposite sign as the disassembly process. Consequently, oligomer dissociation with negative enthalpy also implies that the aggregation process is endothermic and entropically driven (*29, 30*). The reaction enthalpy has three different contributing factors. ΔH_s represents the enthalpy due to the uptake or release of the ordered water molecules from the contact interface (hydration−dehydration phenomena). ΔH_i corresponds to the enthalpic changes from noncovalent interactions such as hydrogen bonding, electrostatic forces, and van der Waals interactions. ΔH_c is related to the conformational enthalpy when an ordered secondary structure of the protein is formed. Considering the unfavorable positive enthalpy value of 2-CysPRX assembly, we conclude that $\Delta H_c + \Delta H_i$ values are exothermic, since protein−protein interaction and protein folding involve favorable (negative) enthalpy (*30*). Therefore, the total endothermic enthalpy of 2-CysPRX dimer binding is attributed to a large unfavorable and thus positive solvation enthalpy due to the release of very ordered water molecules from the monomer−oligomer interface. Protein folding and binding of ligand to protein through hydrophobic interactions are often accompanied by the burial of nonpolar surfaces from water (*36*).

ITC measurements combined with analytic ultracentrifugation have shown that the dimer of interleukin-8 dissociates

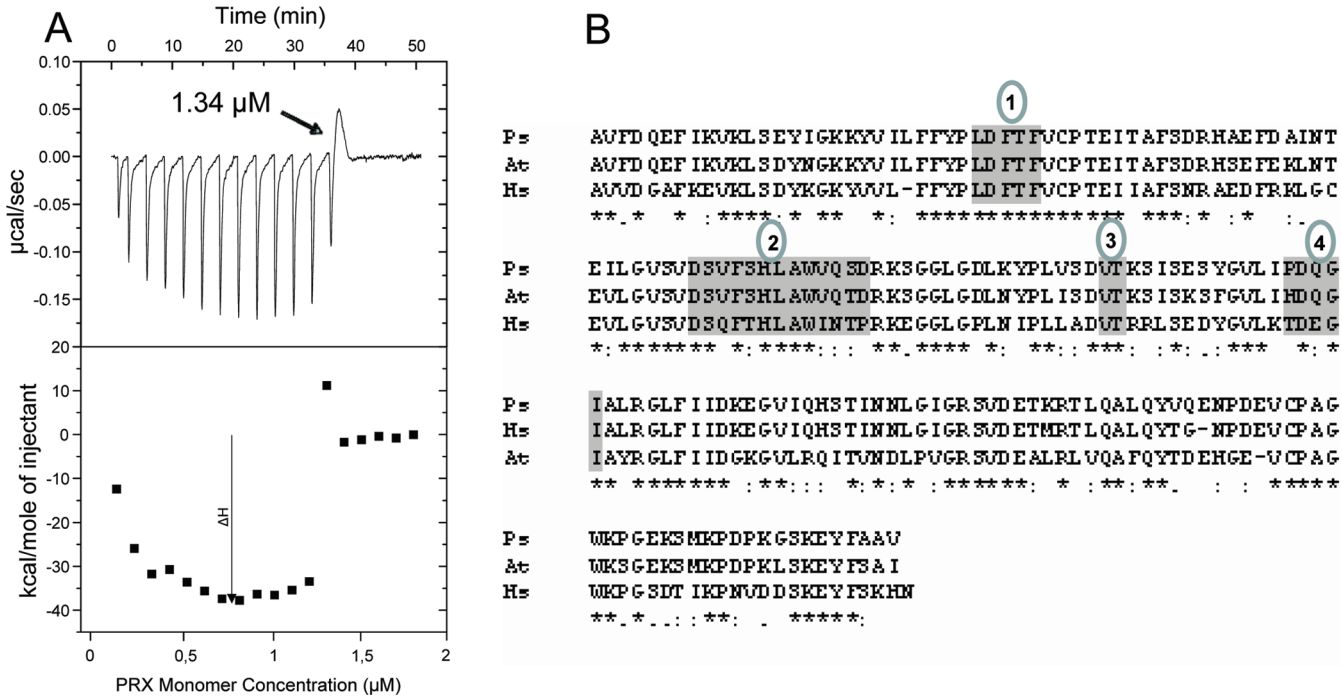

FIGURE 4: Interspecies dimer−decamer interactions. (A) Complementation assay between At-2-CysPRX and human PRDX1 performed by ITC. The thermograms resulted from injection of 91 μM At-2-CysPRX into the cell containing 1 μM PRDX1. Prior to the experiment, the proteins were dialyzed overnight against phosphate buffer (pH 8.0) supplemented with 1 mM DTT. (B) Alignment of amino acid sequences of typical 2-CysPRXs from *P. sativum* (GenBank accession number AJ315851), *A. thaliana* (GenBank accession number Y10478), and *H. sapiens* (GenBank accession number P32119). Regions implicated in the dimer−dimer interface are highlighted in gray and numbered from 1 to 4. Asterisks indicate identical, colons conserved, and periods partly conserved amino acid residues.

to monomers with an equilibrium dissociation constant of 18 μM. Since this value is higher than the physiological concentration, the authors concluded that the monomer was the in vivo predominating and active form (*26*). The 2-CysPRX concentration in the chloroplast was estimated to be >60 μM (*8, 37*). The K_d for disassembly of the decamer−dimer species of 1.58 μM (Figure 2A) indicates that reduced 2-CysPRX usually exists as a decamer in vivo. Interestingly, oxidized and overoxidized PRXs did not generate heat. Oxidized 2-CysPRX is present as a dimer even at high concentrations (Figure 3A) and cannot dissociate after dilution into the buffer. The overoxidized 2-CysPRX apparently adopts an altered structure that stabilizes the decameric form (*12, 15*) and impedes the dissociation. The different property also implies that the reduced decamer and the overoxidized decamer may function in different cell contexts and may interact with different cell structures (*1, 2, 8*). This hypothesis was further confirmed when reduced At-2-CysPRX was injected into the overoxidized form. The number of injections of reduced At-2-CysPRX until cessation of dissociation was unchanged with and without oxidized or overoxidized protein in the buffer.

Under physiological conditions, 2-CysPRX exists mostly as a decamer favored by reducing conditions and high concentrations. At a concentration of >1.58 μM, the reduced dimer concentration is suggested to be unchanged while the reduced decamer concentration increases. This particular behavior could be simulated by the transition model described by eqs 3–8 and was confirmed by the lack of release of heat upon injection of 2-CysPRX above the CTC. The decamers could act as specific redox sensors in cell signaling. Under oxidizing conditions, the decamer breaks down, releasing free dimers with intermolecular disulfide bonds that can be regenerated by redox proteins such as thioredoxin and glutathione. If the oxidation is extreme, the cysteine residues will be oxidized irreversibly to the sulfinic forms and the resulting structure is a stable decamer potentially exerting other functions in cell signaling. The inability of the overoxidized decamer to dissociate proves that the fully reduced and overoxidized decamers are structures that have distinct properties and may serve different functions, e.g., in binding to cell structures such as membrane proteins or enzymes (*8, 38*).

Both the titration experiments (Figure 1) and the addition experiment (Figure 5) revealed a very sharp transition suggesting the involvement of cooperativity effects. Cooperativity typically occurs when numerous weak interactions operate simultaneously (*39*) and control the assembly of relevant proteins such as tubulin and actin. Two molecules that contain a complementary binding site assemble to a larger complex with stability ΔG. Accordingly, two molecules having n complementary binding sites interact to give a complex with a stability greater than $n\Delta G$, and this effect is called positive cooperativity (*40*). Cooperative interactions are influenced by two different factors, enthalpy which is related to the increase in the number of bonds and entropy which indicates the loss of degrees of freedom within the complex and also includes changes in the internal rotation and vibrations of the molecules (*40*). These two factors are related; the increased number of bonds affects the mobility of the molecules. The so-called entropy−enthalpy process is present in many biological interactions, producing a low dependence of ΔG on temperature. All 2-CysPRX dilution experiments under reducing conditions were characterized by a very abrupt transition between dissociation and heat dilution phases. This behavior is not exclusive for PRXs and

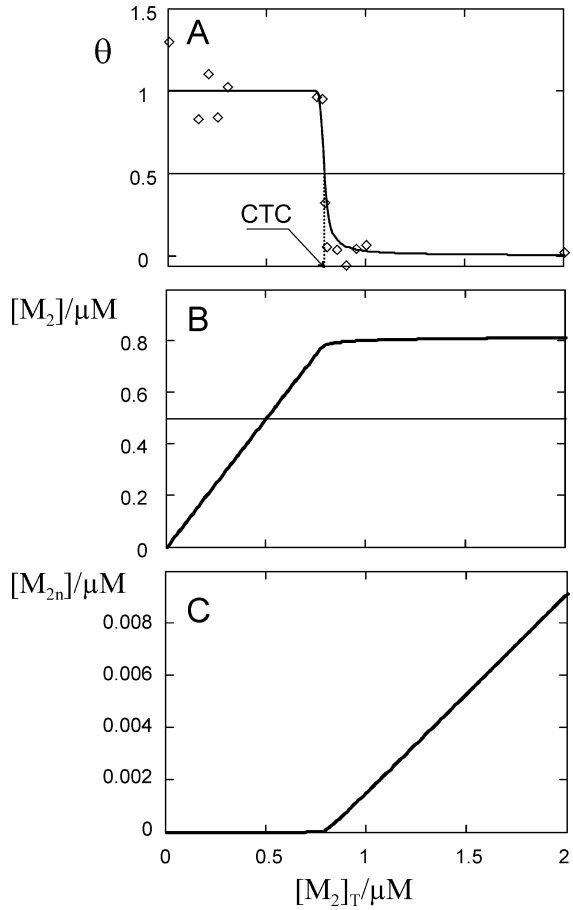

FIGURE 5: 2-CysPRX dissociation in a preloading experiment. (A) Representative thermogram of integrated peak areas (kilocalories per mole) plotted vs the cell concentration of the At-2-CysPRX dimer. At-2-CysPRX was injected in 1.6 μL aliquots from a 50 μM solution in the syringe. Each point corresponds to the average of three independent ITC dilution experiments considering the first four injections (with the exception of the first one) for each assay. The grade θ of the dimer−*n*-dimer transition as a function of the total concentration of dimer ($[M_2]_T$). The points (◇) represent the data on the normalized exothermic heat; the arrow indicates the CTC concentration CTC [$[M_2]_T(\theta = 0.5) = 0.79 \pm 0.1$ μM dimer]. (B) Concentration of free dimers ($[M_2]$) as a function of $[M_2]_T$. (C) Concentration of free *n*-dimers as a function of $[M_2]_T$. The solid lines in panels A−C are the theoretical predictions calculated with eqs 6 and 7 at the dissociation constant $K_d = (2.4 \pm 0.2) \times 10^{-10}$ μM^{n-1} and the stoichiometric coefficient $n = 130 \pm 5$, eluted as indicated.

has been recently described for FtsZ (homologue of tubulin) (*28*), providing information about the possible type of assembly. In principle, we expected to obtain an isodesmic assembly of 2-CysPRXs in which each bond has the same equilibrium constant. Surprisingly, 2-CysPRX assembled in a highly cooperative manner; that is, the decamers were built after formation of an oligomeric nucleus at a determined CTC. The sharp transition cannot be explained by a dissociation model according to eq 1. The reaction scheme (eq 4) for the dissociation of the *n*-dimers into dimers applies in describing the very sharp transition between both molecular species of 2-CysPRX only if the very large stoichiometric coefficient *n* of 130 ± 5 is introduced. Since such high-level aggregation states are not observed, e.g., during gel filtration, the results suggest a highly cooperative nature of the 5-dimer−decamer transition.

The hypothesis of a critical nucleation process is supported by the thermodynamic behavior at the transition concentration, e.g., during titration of wild-type pea 2-CysPRX dissociation (Figure 1). The first injections induced negative peaks up to the 15th injection at 0.84 μM. The 16th injection at 0.9 μM produced an endothermic reaction and initiated the transition. This endothermic phenomenon implies that there is a rapid dissociation upon injection that is followed by a smaller reassociation. The transition was completed at 0.95 μM, after which only heat dilution peaks were observed. The very abrupt transition suggests critical oligomerization concentrations of 1.58 μM for the At-2-CysPRX monomer, 0.9 μM for His-tag free Ps2-CysPRX, and 1.32 μM for Hs-PRDX1. The similarity of the CTC values reveals a significant degree of conservation of this mechanism among the species. It highlights that oligomerization is a typical 2-CysPRX property. Despite the similarity in the CTCs among the PRXs from different species, the complementation assay testing injections of At-2-CysPRX into Ps-2-CysPRX or Hs-PRDX1 revealed that the dimer−dimer interfaces involved in cooperative binding have differentiated during evolution. The similarity of the CTCs despite interface divergence suggests that the dimer−decamer transition is essential for 2-CysPRX function or, in other words, that a functional constraint conserved the dimer−decamer transition with highly similar CTCs despite emerging sequence variation during evolution.

Recently, Cao et al. (*11*) reported that the presence of an N-terminal His tag in human PRDX3 enhances the dodecamer stability after oxidation and decreases the peroxidase activity in comparison with that of its His-tagged free homologue. Our experiments with reduced 2-CysPRXs from different species with and without the His tag (for Ps-2-CysPRX) gave very similar CTCs, confirming that oligomerization of reduced 2-CysPRX takes place at a monomer concentration of <2 μM and is a general property of typical 2-CysPRXs.

REFERENCES

1. Flohé, L., Budde, H., and Hofmann, B. (2003) Peroxiredoxins in antioxidant defense and redox regulation. *Biofactors 19*, 3–10.
2. Dietz, K. J., Jacob, S., Oelze, M. L., Laxa, M., Tognetti, V., de Miranda, S. B., Baier, M., and Finkemeier, I. (2006) The function of peroxiredoxin in plant organelle redox metabolism. *J. Exp. Bot. 57*, 1697–1709.
3. Rouhier, N., and Jacquot, J. P. (2002) Plant peroxiredoxins: Alternative hydroperoxide scavenging enzymes. *Photosynth. Res. 74*, 93–107.
4. Kim, Y. J., Ahn, J. Y., Liang, P., Ip, C., Zhang, Y., and Park, Y. M. (2007) Human Prx1 gene is a target of Nrf2 and is upregulated by hypoxia/reoxigenation: Implication to tumor biology. *Cancer Res. 15*, 546–554.
5. Zhou, Y., Kok, K. H., Chun, A. C., Wong, C. M., Wu, H. W., Lin, M. C., Fung, P. C., Kung, H., and Jin, D. Y. (2000) Mouse peroxiredoxin V is a thioredoxin peroxidase that inhibits p53-induced apoptosis. *Biochem. Biophys. Res. Commun. 268*, 921–927.
6. Kawazu, S., Komaki-Yasuda, K., Oku, H., and Kano, S. (2007) Peroxiredoxins in malaria parasites: Parasitologic aspects. *Parasitology 57*, 1–7.
7. Harris, J. R. (1968) Release of a macromolecular protein component from human erythrocyte ghosts. *Biochim. Biophys. Acta 150*, 535–537.
8. König, J., Baier, M., Horling, F., Kahmann, U., Harris, G., Schürman, P., and Dietz, K. J. (2002) The plant-specific function of 2-Cys peroxiredoxin-mediated detoxification of peroxides in the

redox-hierarchy of photosynthetic electron flux. *Proc. Natl. Acad. Sci. U.S.A. 99*, 5738–5743.
9. Bernier-Villamor, L., Navarro, E., Sevilla, F., and Lazaro, J. J. (2004) Cloning and characterization of a 2-Cys peroxiredoxin from *Pisum sativum*. *J. Exp. Bot. 55*, 2191–2199.
10. Barranco-Medina, S., Krell, T., Finkemeier, I., Sevilla, F., Lázaro, J. J., and Dietz, K. J. (2007) Biochemical and molecular characterization of the mitochondrial peroxiredoxin PsPrxII F from *Pisum sativum*. *Plant Physiol. Biochem. 45*, 729–739.
11. Cao, Z., Bhella, D., and Gordon, L. (2007) Reconstitution of the mitochondrial PrxIII antioxidant defence pathway: General properties and factors affecting PrxIII activity and oligomeric state. *J. Mol. Biol. 372*, 1022–1033.
12. Wood, Z. A., Poole, L. B., Hantgan, R. R., and Karplus, A. (2002) Dimers to doughnuts: Redox-sensitive oligomerization of 2-cysteine peroxiredoxins. *Biochemistry 41*, 5493–5504.
13. Guimaraes, B. G., Souchon, H., Honoré, N., Saint-Joanis, B., Brosch, R., Shepard, W., Cole, S. T., and Alzari, P. M. (2005) Structure and mechanism of the alkyl hydroperoxidase AhpC, a key element of the *Mycobacterium tuberculosis* defense system against oxidative stress. *J. Biol. Chem. 280*, 25725–25742.
14. Hirotsu, S., Abe, Y., Okada, K., Nagahara, N., Hori, H., Nishino, T., and Hakoshhima, T. (1999) Crystal structure of a multifunctional 2-Cys peroxiredoxin heme-binding protein 23 kDa/proliferation associated gene product. *Proc. Natl. Acad. Sci. U.S.A. 96*, 12333–12338.
15. Schroder, E., Littlechild, J. A., Lebedev, A. A., Errington, N., Vagin, A. A., and Isupov, M. N. (2000) Crystal structure of decameric 2-Cys peroxiredoxin from human erythrocytes at 1.7 Å resolution. *Struct. Folding Des. 8*, 605–615.
16. Sarma, G. N., Nickel, C., Rahlfs, S., Fischer, M., Becker, K., and Karplus, P. A. (2005) Crystal structure of a novel *Plasmodium falciparum* 1-Cys peroxiredoxin. *J. Mol. Biol. 346*, 1021–1034.
17. Dietz, K. J. (2003) Plant peroxiredoxins. *Annu. Rev. Plant Biol. 54*, 93–107.
18. Echalier, A., Trivelli, X., Corbier, C., Rouhier, N., Walker, O., Tsan, P., Jacquot, J. P., Aubry, A., Krimm, I., and Lancelin, J. M. (2005) Crystal structure and solution NMR dynamics of a D (type II) peroxiredoxin glutaredoxin and thioredoxin dependent: A new insight into de peroxiredoxin oligomerism. *Biochemistry 44*, 1755–1767.
19. Kitano, K., Niimura, Y., Nishiyama, Y., and Miki, K. (1999) Stimulation of peroxidase activity by decamerization related to ionic strength: AhpC protein from *Amphibacillus xylanus*. *J. Biochem. 126*, 313–319.
20. Kristensen, P., Rasmussen, D. E., and Kristensen, B. I. (1999) Properties of thiol-specific anti-oxidant protein or calpromotin in solution. *Biochem. Biophys. Res. Commun. 262*, 127–131.
21. Chauhan, R., and Mande, S. C. (2001) Characterization of the *Mycobacterium tuberculosis* H37Rv alkyl hydroperoxidase AhpC points to the importance of ionic interactions in oligomerization and activity. *Biochem. J. 354*, 209–215.
22. Schröder, E., Willis, A. C., and Ponting, C. P. (1998) Porcine natural-killer-enhancing factor-B: Oligomerization and identification as a calpain substrate in vitro. *Biochim. Biophys. Acta 1383*, 279–291.
23. Pierce, M. M., Raman, C. S., and Nall, B. T. (1999) Isothermal titration calorimetry of protein-protein interactions. *Methods 19*, 213–221.
24. Velázquez-Campoy, A., and Freire, E. (2005) ITC in the post-genomic era. .? Priceless. *Biophys. Chem. 115*, 115–124.
25. Naghibi, H., Tamura, T., and Sturtevant, J. M. (1995) Significant discrepancies between van't Hoff and calorimetric enthalpies. *Proc. Natl. Acad. Sci. U.S.A. 92*, 5597–5599.
26. Burrows, S. D., Doyle, M. L., Murphy, K. P., Franklin, S. G., White, J. R., Brooks, I., McNulty, D. E., Scott, M. O., Knutson, J. R., Porter, D., Young, P. R., and Hensley, P. (1994) Determination of the monomer-dimer equilibrium of interleukin-8 reveals it is a monomer at physiological concentrations. *Biochemistry 33*, 12741–12745.
27. Lovatt, M., Cooper, A., and Camilleri, P. (1996) Energetic of cyclodextrin-induced dissociation of insulin. *Eur. Biophys. J. 24*, 354–357.
28. Caplan, M. R., and Erickson, H. P. (2003) Apparent cooperative assembly of the bacterial cell division protein FtsZ demonstrated by isothermal titration calorimetry. *J. Biol. Chem. 278*, 13784–13788.
29. Luke, K., Apiyo, D., and Wittung-Stafshede, P. (2005) Dissecting homo-heptamer thermodynamics by isothermal titration calorimetry: Entropy-driven sssembly of co-chaperonin protein 10. *Biophys. J. 89*, 3332–3336.
30. Lakshminarayanan, R., Fan, D., Du, C., and Moradian-Oldak, J. (2007) The role of secondary structure in the entropically driven amelogenin self-assembly. *Biophys. J. 107, 93*, 3664–3674.
31. Velazquez-Campoy, A., Leavitt, S., and Freire, E. (2004) Characterization of protein-protein interactions in isothermal titration calorimetry. *Methods Mol. Biol. 261*, 35–54.
32. König, J., Lotte, K., Plessow, R., Brockninke, A., Baier, M., and Dietz, K. J. (2003) Reaction mechanism of plant 2-Cys Peroxiredoxin. Role of the C terminus and the quaternary structure. *J. Biol. Chem. 278*, 24409–24420.
33. Heerklotz, H., and Seeling, J. (2000) Titration calorimetry of surfactant-membrane partitioning and membrane solubilization. *Biochim. Biophys. Acta 1508*, 69–85.
34. Crowley, P. B., and Golovin, A. (2005) Cation-π Interactions in protein-protein interfaces. *Proteins: Struct., Funct., Bioinf. 59*, 231–239.
35. Parsonage, D., Youngblood, D. S., Sarma, G. N., Wood, Z. A., Karplus, P. A., and Poole, L. B. (2005) Analysis of the link between enzymatic activity and oligomeric state in AhpC, a bacterial peroxiredoxin. *Biochemistry 44*, 10583–10592.
36. Eftink, M., and Biltonen, R. (1980) Thermodynamics of interacting biological systems. In *Biological Microcalorimetry* (Beezer, A. E., Ed.) pp 343−412, Academic Press, London.
37. Peltier, J. B., Cai, Y., Sun, Q., Zabrouskov, V., Giacomelli, L., Rudella, A., Ytterberg, A. J., Rutschow, H., and van Wijk, K. J. (2006) The oligomeric stromal proteome of *Arabidopsis thaliana* chloroplasts. *Mol. Cell. Proteomics 5*, 114–133.
38. Caporaletti, D., D'Alessio, A. C., Rodriguez-Suarez, R. J., Senn, A. M., Duek, P. D., and Wolosiuk, R. A. (2007) *Biochem. Biophys. Res. Commun. 355*, 722–727.
39. Williams, D. H., Maguire, A. J., Tsuzuki, W., and Westwell, M. S. (1998) An Analysis of the Origins of a Cooperative Binding Energy of Dimerization. *Science 280*, 711–714.
40. Camara-Campos, A., Hunter, C. A., and Tomas, S. (2006) Cooperativity in the self-assembly of porphyrin ladders. *Proc. Natl. Acad. Sci. U.S.A. 103*, 2034–3038.

BI8002956